Anomalous Group velocity and Plasma Dispersion in the Laser Wakefield Accelerator through a new Relativistic Theory

J. Yazdanpanah

The Plasma Physics and Fusion Research School, Tehran, Iran

ABSTRACT

A new cold relativistic theory is proposed to describe the Laser WakeField Accelerator (LWFA) in the presence of pulse evolutions, capable of being utilized to study the group velocity and the plasma dispersion. This new capability is mainly due to exploiting the concept of the real Lorentz-boost Pulse Co-Moving (LPCM) frame, in spite of previous studies. The theory is reduced to the well-known Quasi-Static Approximation (QSA) in the absence of the pulse evolutions, and shows excellent agreement with Particle-In-Cell (PIC) simulations in terms of its new results. The obtained results show the extremely extra-ordinary nature of the fully nonlinear plasma physics of LWFA. It is turned out that the local group and phase velocities of the light are approximately equal. The obtained group-velocity evolves in time according to $\beta_g = \sin[\tan^{-1}(-t/\tau_0 + \alpha)]$ (τ_0 and α are parameters depending on wake amplitude and initial group velocity) at early stages, showing non-explicit density dependency and remaining above the linear value over a long period of the propagation. The obtained equations for the carrier-mode, on the other hand, consistently suggest the emergence of a new dispersion

branch with the linear relation $\omega \approx ck$ (c is the light speed). Regarding these remarks, we expend on the plasma dispersion in details with the aid of simulations, confirming the observed anomalies and the emergence of the new branch. In addition, a detailed description of the spectral evolutions in the dispersion plan is provided and it is shown that the dispersion anomalies tend to cease at long pulse lengths.

I. INTRODUCTION

Inspired by the rapid developments in the technology of ultra-intense ultra-short pulse lasers, the Laser Wake-Field Accelerator (LWFA) has received increasing interests over the past two decades (see e.g. Refs. [1, 2] and references therein). In the LWFA the laser-induced relativistic, ultra-high phase-velocity electron plasma waves are utilized to accelerate the self-injected electron bunches to ultra-high energies. The performance of this accelerator crucially depends on the plasma wave phase velocity behind the pulse dependent on the pulse group velocity [2], and the nonlinear pulse evolutions [3]. These nonlinear evolutions [3-10] are also fundamental to the plasma heating and particle acceleration in interactions with high density plasmas [11-14].

Many nonlinear aspects of the pulse evolution have been studied using the so-called Slow Envelope Analyses (SEA) firstly proposed in [4]. It is currently well-

known that the laser pulse experiences nonlinear depletion and deceleration due to the wake excitation [4, 5]. Also, it has been demonstrated that the nonlinear wakefield interactions lead to pulse compression [6-7] and amplitude-amplification accompanied by the wakefield amplification [6]. More recently, theoretical and numerical studies have indicated that the problem shows new complexities. The plasma-wave phase-velocity decreases behind the pulse due to the wakefield amplification [3] and the pulse length shows intricate evolutions at long times, resulting in multi-phase wakefiled variations and the eventual wake destructions [8]. In addition, the multi-dimensional extension of the theory has been considered in the plasma channel [9] and the local details of pulse evolutions has been investigated using a photon-kinetic approach [10]. However, despite to these extensive studies, some important issues like the pulse group velocity and the plasma dispersion have remained very poorly understood. The pulse group-velocity is very important to LWFA (see e. g. [3]), in relation with description of the plasma-wave phase velocity necessary to estimate the maximum attainable acceleration. The plasma dispersion is directly relevant to this issue and is extremely complex in the fully nonlinear regime. The most important previous work on the topic of group velocity, Ref. [15], calculates this quantity as *the rate of the total-energy transport* and *not the rate of radiation energy transport*. This

calculation is of less interest in LWFA, as, the relation between the obtained group velocity and the plasma-wave phase-velocity remains lacking.

The existing SAE approach [4], used in the previous studies [3-10], suffers from some discrepancies and is inadequate to calculate the pulse group velocity and reproduce the correct plasma dispersion. SEA presumes the wave solution in the form of $\psi(x,t)=\hat{\psi}(\xi,t)\exp(-i\omega_0 t+ik_0 x)$. Here $\xi\equiv x-v_g^0 t$, $v_g^0\equiv ck_0/\omega_0$ is the constant linear group velocity and ω_0 and k_0 are respectively the carrier frequency and wave-number obeying the linear dispersion relation $\omega_L^2(k)=c^2k^2+\omega_p^2$. Here, $\omega_p=(n_{e0}e^2/\varepsilon_0 m_e)^{1/2}$ is the plasma frequency and c is the light speed, and n_{e0}, e, ε_0 and m_e are respectively the undisturbed plasma density, the elementary charge, the vacuum permittivity and the electron mass. The envelope function $\hat{\psi}(\xi,t)$ is supposed to vary very slowly with time, such that we have $\partial\hat{\psi}/\partial t << c\partial\hat{\psi}/\partial\xi\approx ck_p\hat{\psi}=\omega_p\hat{\psi}$ $(k_p=\omega_p/c)$. However, difficulties arise concerning this approach; firstly, it is immediately found that despite the expectations, SEA does not reduce to the well known Quasi-Static Approximation (QSA) described e.g. in [16] under the ignorance of the time-variations in the envelope function, $\hat{\psi}(\xi,t)$ -in the phasor term, the individual time and space dependencies cannot be completely eliminated in terms of the variable ξ. Deeper

examinations reveals another problem; the slow envelope variations implies the pulse carrier-frequency to remain very close to its initial value during the propagation, i.e. we should have $\omega_0(t) \approx \omega_0(0) + \delta\omega(t)$ with $\delta\omega << \omega_p$. This implication highly restricts the time-scope of SEA, as the radiation experiences strong redshift due to the pulse deceleration (see e.g. [3, 4, 5, 8]). It will be soon observed in our simulations that it takes not very long for the redshift to reach the values comparable to the initial laser frequency, causing the early-time breakdown of $\delta\omega << \omega_p$.

The discrepancies outlined above in relation with SEA are of two main origins; the first origin is the tacit generalization of the linear paradigms into the fully non-linear regime in the case of plasma dispersion. The second source is the improper relativistic treatment of the problem, mainly related to the ill-definition and unsophisticated application of the concept of the Pulse Co-Moving (PCM) frame. It has been commonly believed that the Pulse Co-Moving (PCM) frame is not a real Lorentz frame but it only bears some algebraic transformation (see e.g. [16]). This belief may have prevented from treatments based on the zero or slow pulse evolutions in the *real* Lorentz boost Pulse Co-Moving frame. It will be soon clear in this work that such treatments can produce the correct plasma dispersion and

automatically take into account the group velocity variations and the resultant carrier-frequency evolutions.

In this paper, a new cold relativistic theory (in one space -three velocity dimensions and for p-polarized laser pulse) is proposed to describe the Laser WakeField Accelerator (LWFA) in the presence of pulse evolutions, capable of being utilized to study the group velocity and the plasma dispersion. This capability is mainly due to exploiting the concept of the real Lorentz-boost Pulse Co-Moving (LPCM) frame, in spite of the previous studies. LPCM frame, moves with the global pulse group velocity and differs from the PCM frame commonly used (see e.g. [16]) as an unreal frame in the well-known Quasi-Static Approximation (QSA). Upon the ignorance of pulse evolutions in the LPCM, our results reduce to those of QSA. Otherwise, local equations are obtained for the nonlinear pulse evolutions. The obtained results are successfully examined against the Particle-In-Cell (PIC) simulations and show the extremely extra-ordinary nature of the fully nonlinear plasma physics of LWFA. It is turned out that the local group and phase velocities of the light are approximately equal. This equality, in the absence of the depletion, results in the detailed (not cycle-averaged) energy conservation in the LPCM frame, producing the common Hamiltonian-constant in the laboratory frame used in QSA. The obtained group-velocity evolves in time

according to $\beta_g = \sin[\tan^{-1}(-t/\tau_0 + \alpha)]$ (τ_0 and α are parameters depending on wake amplitude and initial group velocity) at early stages, showing non-explicit density dependency and remaining above the linear value over a long period of the propagation. The obtained equations for the carrier-mode, on the other hand, consistently suggest the emergence of a new dispersion branch with the linear relation $\omega \approx ck$ (c is the light speed). Regarding these remarks, we expend on the plasma dispersion in details with the aid of simulations, confirming the observed anomalies and the emergence of the new branch. In addition, a detailed description of the spectral evolutions in the dispersion plan is provided and it is shown that the dispersion anomalies tend to cease at long pulse lengths.

This paper is organized in different sections. In Sec. II the governing equations are briefly outlined together with our approach bases. In Sec. III, our approach is examined against the common QSA. In Sec. IV the theory of the interaction in the presence of pulse evolutions is outlined and is examined against the simulations. A complementary section (Sec. V) is devoted to discuss the observed anomalies by expanding on the plasma dispersion. Finally, the paper is concluded in Sec. VI.

II. GOVERNING EQUATIONS

The basic applied equations are the well known set of cold fluid equations plus Maxwell equations, remaining covariant among different reference frames,

$$\frac{\partial n_q}{\partial t}+\nabla\cdot\left(n_q\mathbf{v}_q\right)=0 \tag{1a}$$

$$\frac{\partial[\mathbf{p}_q+Q_q\mathbf{A}]}{\partial t}=-\nabla(m_qc^2\gamma_q-e\phi) \tag{1b}$$

$$\frac{\partial^2\phi}{\partial x^2}+\frac{\partial}{\partial t}\left(\nabla\cdot\mathbf{A}\right)=-\frac{1}{\varepsilon_0}\sum_q n_qQ_q \tag{1c}$$

$$\frac{\partial^2\mathbf{A}}{c^2\partial t^2}-\frac{\partial^2\mathbf{A}}{\partial x^2}+\nabla\left(\nabla\cdot\mathbf{A}+\frac{1}{c^2}\frac{\partial\phi}{\partial t}\right)=\frac{1}{\varepsilon_0c^2}\sum_q n_qQ_q\mathbf{v}_q \tag{1d}$$

Here, n, $\mathbf{p}$, Q, ϕ and $\mathbf{A}$ stand for density, momentum, electric charge, scalar potential and vector potential, respectively. The subscript q indicates that the quantities are correspond to the component q^{th} (electron or ion) of the plasma. $\mathbf{v}_q=\mathbf{p}_q/m_q\gamma_q$ and $\gamma_q=(1-\mathbf{v}_q.\mathbf{v}_q/c^2)^{-1/2}$ are the velocity and the relativistic gamma factor, respectively. The Coulomb gauge is applied on potentials *in the laboratory frame*, i.e. for each desired frame we transform the laboratory equation $\nabla\cdot\mathbf{A}=0$ to that frame using Lorentz transformations. Also the analyses are restricted to a one spatial dimension, say *x,* the direction of the laser propagation.

It is shown in a supplementary material (A) that the set of equations (1) result in the following covariant conservations laws [17],

$$\frac{\partial u_{EM}}{\partial t}+m_ec^2\frac{\partial\gamma_en_e}{\partial t}+c^2\frac{\partial g_x}{\partial x}+m_ec^2\frac{\partial\gamma_en_ev_{ex}}{\partial x}=-en_i\mathbf{v}_i\cdot\mathbf{E}\,, \tag{2a}$$

$$\frac{\partial g_x}{\partial t} + m_e \frac{\partial \gamma_e n_e v_{ex}}{\partial t} + \varepsilon_0 \frac{\partial}{\partial x}[\frac{1}{2}E_y^2 + \frac{1}{2}c^2 B_z^2 - \frac{1}{2}E_x^2] + m_e \frac{\partial \gamma_e n_e v_{ex}^2}{\partial x} = -en_i[E_x + v_{iy}B_z] \quad (2b)$$

where subscripts e and i are respectively used for electrons and ions of a hydrogen type plasma. x and y are respectively the propagation and the polarization directions. $u_{em} = \varepsilon_0(E^2 + c^2B^2)/2$ and $\mathbf{g} = \varepsilon_0 \mathbf{E} \times \mathbf{B}$ are the electromagnetic energy and momentum respectively ($\mathbf{E}$ and $\mathbf{B}$ are electric and magnetic fields respectively). We can neglect the contribution of $v_{iy}B_z$ compared to E_x in the right hand side of (2b), because due to their heavy mass, ions remain approximately immobile in the direction of the laser polarization. The derivation is based on the general, local conservation laws already summarized in text books listed in the supplemental material.

The idea is to solve the set of Eqs. (1) and (2) in the LPCM frame using the simplifying facts of zero or very slow time variations in this frame, and then transform the results back into the laboratory frame.

III. REDUCTION TO THE QSA

The QSA has been has been extensively considered in the previous LWFA studies (see e.g. [2]) in order to obtain a closed solution to equations (1a-1d). The main assumption of the model is that the laser pulse is invariant in its commoving frame moving with a *constant* group velocity, v_g. In this way the explicit solution of the wave equation (1d) is avoided and the net effect of this equation is assumed

to be only in applying $v_g \neq c$. With these regards, QSA implies that the time-space dependencies in the laboratory frame appear in the combination $x - v_g t$.

Regarding the QSA, it has been frequently stated that the pulse commoving frame is not a new real Lorentz-boost frame but it is just the laboratory frame bearing some algebraic transformations (see e.g. [16]). This definition of the frame is both false and misleading. In this section, we present a new approach to QSA, based on application of equations (1a-1c) inside the real Lorentz-boost pulse commoving frame in the presence of time-independency in this frame. In this way, the encountered ambiguity is clarified and new important insights are obtained.

In a separate supplemental material (B), we have presented a detailed proof supporting the statement that the common QSA equations could be obtained by assuming the time-independency in the *real,* Lorentz-boost Pulse Co-Moving (LPCM) frame and then transforming the reduced equations into the laboratory [18]. The time-independency results from the pulse invariance in its commoving frame. The proof for this statement is straightforward but space-wasting. It can be easily realized by noting that the time-independency in the LPCM frame means that quantities are only functions of $x\big|_{PCM}$. Since, according to the Lorentz transformations, $x\big|_{PCM} = \gamma_g (x - v_g t)$, time-space dependencies in the laboratory frame appear in the combination $\xi \equiv x - v_g t$ (note γ_g is a constant in QSA) as

assumed in the common QSA solutions. Here $\gamma_g = (1 - v_g^2 / c^2)^{-1/2}$ is the relativistic factor of the LPCM frame and the notation $X\big|_{PCM}$ indicates that X is measured in the LPCM frame. Hereafter, this indication will be made for the LPCM quantities and no special indication will be made on the laboratory quantities. In this section, the statement proof is briefly followed and the main points of QSA, necessary for paper consistency, are given.

Since quantities are assumed time-independent in the LPCM frame, solution of Eqs. (1a-1b) in this frame (putting $\partial / \partial t = 0$ in these equation) results in the conserved particle flux and energy,

$$[n_e v_{ex}]\big|_{PCM} = -v_g \gamma_g n_{e0}, \tag{3a}$$

$$[\gamma_e m_e c^2 - e\phi]\big|_{PCM} = \gamma_g m_e c^2. \tag{3b}$$

In the right hand sides of Eqs. (3a-3b) we have used the fact that the undisturbed-plasma flows toward the pulse region with velocity $-v_g$ in the LPCM frame. In (3a), we have also used the relation $n_{e0}\big|_{PCM} = \gamma_g n_{e0}$ for the undisturbed electron density in the LPCM frame. It can be easily shown [18], using the Lorentz transformations, that the equations (3a-3b) are respectively equivalent to the following well-known QSA constants already outlined in the literatures (see e. g. [2, 16]):

$$n_e(\beta_g - \beta_{ex}) = n_{e0}\beta_g , \tag{3c}$$

$$\gamma_e m_e c^2 (1 - \beta_g \beta_{ex}) - e\phi = m_e c^2 \tag{3d}$$

where $\beta_g \equiv v_g / c$ and $\boldsymbol{\beta}_e \equiv \mathbf{v}_e / c$.

Other QSA equations are obtained straightforwardly as well as Eqs. (3). For example we obtained $\left[\gamma_e \beta_{ey} = a_y\right]\Big|_{PCM} (\mathbf{a} \equiv e\mathbf{A} / m_e c)$ which transforms to the conservation of the transverse canonical momentum, $\gamma_e \beta_{ey} = a_y$, in the laboratory frame. Afterward, the procedure of solving the governing equations is the same as the previous literatures; using the equation $\gamma_e \beta_{ey} = a_y$ together with Eqs. (3), the right hand side of the Poisson equation (1c) is expressed in terms of ϕ. The resultant equation is then integrated to give the electric field and the electric potential in the disturbed region. Behind the pulse, $a_y = 0$ and this procedure produces a first integral,

$$E_x^2 + 2(\gamma_e - 1)E_p^2 = E_w^2 \tag{4}$$

where $E_p = m_e c\omega_p / e$ and E_w is the wakefield amplitude.

The contents of this section not only prove the equivalence of our approach with the common QSA, in the absence of pulse depletion, but also they bear an important physical insight. The Hamiltonian constant (3b) would not be derived unless we have assumed that LPCM time-independency holds about all

components of the vector potential including the transverse component A_y, as well as other quantities, i.e. $[\partial \mathbf{A} / \partial t = 0]\big|_{PCM}$. The situation would not change even if we have considered only the *x*-component of Eq. (1b), as we covariantly have $\gamma_e = (1 + p_x^2 / m_e^2 c^2 + a_y^2)^2$. Satisfaction of $[\partial A_y / \partial t = 0]\big|_{PCM}$ implies the equality of the light phase-velocity with its group-velocity (the carrier-frequency vanishes in the LPCM frame). This phenomenon makes a radical difference with the linear theory which predicts that the light phase velocity is always larger than its group velocity, and will be fully expanded along with our future discussions. The encountered conflict with the linear theory may seem to be circumvented by assuming the cycle- averaged version of (1b) in the presence of A_y oscillations in LPCM. However, at the best, this approach results in a cycle-averaged Hamiltonian-constant (not instantaneous constant) which as will be soon clear, contradicts with the direct PIC simulations.

IV. INTERACTION IN THE PRESENCE OF PULSE EVOLUTIONS

A. THE MODEL DESCRIPTION

In this section we consider the LWFA in the presence of pulse evolutions, postulating very slow pulse and plasma variations in the LPCM frame -in the sense that the pulse and the plasma remain approximately invariant during a small time period which is still sufficient for the plasma to pass a plasma wavelengths in the

LPCM frame. Since the plasma wavelength is proportional to c/ω_p, the postulated assumption means that the time-scale of evolutions in the LPCM frame is very longer than ω_p^{-1}. With this assumption, it is expected that the equality between the group and phase velocities of the pulse, outlined in the previous section, be locally preserved. In addition the slow phase-velocity (phase) modulations originated from the local nature of interaction are un-important, as the solutions of Eqs (1a-1c) in the LPCM frame does not show high sensitivity to small changes in the plasma wave phase velocity, as long as the maximum plasma velocity does not get very close to the phase velocity (wave break conditions [2]). It is clear that despite to SEA, the proposed assumption do not necessitate ignoring the carrier-frequency (wave-number) variations as it does not limit the global pulse deceleration (variations of LPCM velocity).

Under the established assumptions, the set of equations (3a-3b) remains approximately valid about the plasma. In addition, we can set in equations (2a) and (2b), $\partial\gamma_e n_e/\partial t\big|_{PCM}\approx 0$, $\partial\gamma_e n_e v_{ex}/\partial t\big|_{PCM}\approx 0$, $\partial\phi/\partial t\big|_{PCM}\approx 0$ and $\partial A_x/\partial t\big|_{PCM}\approx 0$ (note that $A_x\big|_{PCM}=-\gamma_g\beta_g\phi/c=-\beta_g\,\phi\big|_{PCM}/c$ due to the gauge condition $A_x=0$ in the laboratory frame) . And by applying these simplifications we obtain respectively from (2a) and (2b),

$$\{\frac{\partial u_{EMT}}{\partial t}+\frac{\partial}{\partial x}[c^2 g_x - n_{e0}m_e c^2\gamma_g v_g\gamma_e + n_{e0}e\gamma_g v_g\phi]=0\}\Big|_{PCM}, \quad (5a)$$

$$\{\frac{\partial g_x}{\partial t}+\frac{\partial}{\partial x}[\frac{\varepsilon_0}{2}E_y^2+\frac{\varepsilon_0}{2}c^2B_z^2-\frac{\varepsilon_0}{2}E_x^2-n_{e0}m_e v_g\gamma_g\gamma_e v_{ex}-en_{e0}\gamma_g\phi]=0\}\Big|_{PCM} \quad (5b)$$

where we have made use of Eq. (3a), $\mathbf{E}=-\nabla\phi-\partial\mathbf{A}/\partial t$ and the facts that $v_{ix}\big|_{PCM}\approx -v_g$ and $n_i\big|_{PCM}\approx\gamma_g n_{e0}$ due to the heavy ion mass. u_{EMT} is defined to be $u_{EMT}=\varepsilon_0(E_\perp^2+c^2B_\perp^2)/2$. The second term in the right hand side of Eq. (2b) has been neglected in arriving to Eq. (5b) according to arguments given below Eq. (2b).

Eq. (5a) can be further simplified by using equation (3b) and gives,

$$\{\frac{\partial u_{EMT}}{\partial t}+c^2\frac{\partial g_x}{\partial x}=0\}\Big|_{PCM}. \quad (6a)$$

This equation describes the energy conservative light flow through a self-consistent density profile. It is consistent with the fact that the plasma mechanical-energy and more generally the plasma profile does not vary with time in the LPCM frame.

By eliminating ϕ in Eq. (5b) using Eq. (3b), and applying the Lorentz transformations $E_x=E_x\big|_{PCM}$ and $\gamma_e=\gamma_e\gamma_g(1+v_g v_{ex}/c^2)\big|_{PCM}$ in the obtained result, equation (5b) reads as,

$$\{\frac{\partial g_x}{\partial t}+\frac{\partial u_{EMT}}{\partial x}=\varepsilon_0 E_p^2\frac{\partial C_W}{\partial x}\}\Big|_{PCM} \quad (6b)$$

Here, $C_w \equiv (E_x / E_p)^2 + 2(\gamma_e - 1)$ is the local normalized wake energy (the local magnitude of wake amplitude) and its gradient shows the local wake excitation. It varies inside the pulse and reaches the constant value of $(E_w / E_p)^2$ behind the pulse (see Eq. 4). Eq. (6b) states that the local light-momentum varies with time due to the convection ($-\partial u_{EMT} / \partial x$ term) and the wake excitation ($E_p^2 \partial C_W / \partial x$ term). The overall effect of the convection term is zero. Therefore, it does not affect the overall depletion and the spectrum evolutions. Equations (6a) together with Eq. (6b) suggests that C_W (albeit with reverse sign) acts as an local effective potential for radiation.

The overall variations of the wave momentum and energy are obtained by integration of Eqs. (6a) and (6b) over x. In this way, we obtain in the LPCM frame,

$$\left.\frac{dH_{FT}}{dt}\right|_{PCM} = 0, \tag{7a}$$

$$\left.\frac{dK_F}{dt}\right|_{PCM} = -\frac{1}{2}\varepsilon_0 E_w^2 \tag{7b}$$

where $H_{FT} = \int_{-\infty}^{\infty} \mathrm{d}x u_{EMT}$ and $\mathbf{K}_F = \int_{-\infty}^{\infty} \mathrm{d}x \mathbf{g}$ are the total electromagnetic energy and momentum respectively.

B. THE EARLY TIME EVOLUTIONS AND THE ANOMALOUS GROUP VELOCITY BEHAVIORS

Under the condition $K_F\big|_{PCM}=0$ a full similarity is recovered between the obtained Eqs (7a) and (7b) and those of an ordinary relativistic particle. However, this condition does not hold generally. In particular, the local nature of interaction, expressed in Eqs. (6a) and (6b) by the space dependence of $\partial C_W / \partial x$, implies the radiation phase-modulation and hence nonzero (though very small) radiation evolutions in the LPCM frame. Nevertheless, the carrier-frequency is initially zero in the LPCM frame, therefore, evolutions in the LPCM are very slow and the condition $K_F\big|_{PCM}=0$ holds at least at early times.

Analogous to the relativistic dynamics of an ordinary particle, under the above conditions, the energy (H_{FT}) and the momentum $(\mathbf{K}_F)$ form a four-vector [19], say $\mathbf{K}_4$, which can be written in the covariant form of $\mathbf{K}_4 \equiv (H_{FT}, c\mathbf{K}_F) = H_0(\gamma_g, \gamma_g \mathbf{v}_g)$. Here $\mathbf{v}_g$ is the global electromagnetic group velocity,

$$\mathbf{v}_g = \frac{c^2 \mathbf{K}_F}{H_{FT}}, \tag{8}$$

and $H_0 \equiv H_F\big|_{PCM}$ is the electromagnetic energy in LPCM frame. $\mathbf{v}_g$ has been implicitly used at prior in this paper in defining the LPCM frame. Its relation (8)

gives *the rate of radiation energy transport*, despite the corresponding definition in [15]. H_0 takes the role of the particle rest mass satisfying $dH_0 / d\tau = 0$ (Eq. (7a)), with $\tau \equiv (t)\big|_{PCM}$ being the proper time. Therefore, analogous to the relativistic particle dynamic [19], we can readily apply (7b) in the laboratory frame, i.e.

$$\frac{dK_F}{dt} = -\frac{1}{2}\varepsilon_0 E_w^2 . \tag{9a}$$

We should notify that Eq. (9a) has been obtained and used previously in Ref. [8] via SEA. The reason for this accidental coincidence, despite to the outlined essential difference between our approach and SEA (see the introduction), is that the force term (right hand side of (9a)) has not explicit dependencies on the pulse parameters. Nevertheless, our approach still gains over the SEA, at least, by two reasons. Firstly, the physics is modeled correctly here, with more clarified assumptions and restrictions. Secondly, and more importantly, we can go further and calculate the global group velocity, as we have the relation between the radiation energy and momentum.

Using $c\mathbf{K}_F = H_0 \gamma_g \mathbf{v}_g$ from $\mathbf{K}_4$ presentation, the identity $d[\gamma_g \beta_g] / dt = \gamma_g^3 d\beta_g / dt$ ($\beta_g = v_g / c$) and noting the constancy of H_0, Eq. (9a) takes the form of,

$$\frac{d\beta_g}{dt} = -\frac{1}{2}\frac{\varepsilon_0 c \gamma_{g0} E_w^2}{\gamma_g^3 U_{P0}} . \tag{9b}$$

Here, $U_{p0} = \gamma_{g0} H_0$ is the initial pulse energy and γ_{g0} is the initial group-velocity gamma-factor. Equation (9b), derived for the first time in this work, fully describe the pulse evolutions at the early stages. It states that the pulse is slowly decelerated and loses its energy. Due to the deceleration, the pulse energy in the laboratory frame decreases with time despite to energy conservation in the LPCM frame. When the evolutions of the wake amplitude, E_w, are ignored, for example at initial times, the solution of Eq. (9b) is obtained in the form,

$$\beta_g = \sin[\tan^{-1}(-\frac{t}{\tau_0} + \alpha)], \qquad (9c)$$

where $\tau_0 \equiv 2U_{P0} / \varepsilon_0 c \gamma_{g0} E_w^2$ and $\alpha \equiv \tan[\sin^{-1}[\beta_{g0}]]$. With this solution the depletion time is given by $\tau_d = \alpha \tau_0$ (when $\beta_g = 0$) which differs from previous estimates [3,4] in the way that it takes into account the near c being of the initial group velocity. This difference has been previously observed in PIC simulations of Ref. [6]. Moreover, it is noticed that despite to the linear group velocity, the obtained result (9c) does not show the explicit density dependency. Also, because $\beta_{g0} \approx 1$ (the pulse is initiated in the vacuum) and $\gamma_{g0} >> 1$, α and $\omega_p \tau_d$ tend to very large values. Therefore, due to very smooth variations of $\tan^{-1}$ at its large arguments it is expected that β_g reaches the linear value,

$v_g^0 / c \equiv ck_0 / \omega_{0L} = \sqrt{1 - n_{e0} / n_c}$ after a very long time. This phenomenon will be further discussed in the next section.

An important feature of the pulse evolutions is the temporal variations of the carrier frequency and wave-number, $\omega_0(t)$ and $k_0(t)$. The equality between the local phase-velocities of the plasma-wave and the laser-pulse implies the light frequency to be approximately zero in each local phase frame of the radiation. In early times, in the absence of the phase modulation, every local frame in the radiation region moves approximately with the same velocity as the global LPCM frame, therefore we will have $[\omega_0 \approx 0]\big|_{PCM}$. With this equation, simple expressions can obtained for $\omega_0(t)$ and $k_0(t)$ via Lorentz transformations, i.e. $\omega_0 \approx \gamma_g \beta_g c(k_0\big|_{PCM})$ and $k_0 \approx \gamma_g (k_0\big|_{PCM})$ where $k_0\big|_{PCM}$ remains constant ($k_0(t)\big|_{PCM} = k_0(0)\big|_{PCM}$), and we obtain,

$$\omega_0(t) = \frac{\gamma_g \beta_g}{\gamma_{g0} \beta_{g0}} \omega_0(t=0),\ \mathbf{k}_0(t) = \frac{\gamma_g}{\gamma_{g0}} \mathbf{k}_0(t=0). \qquad (10)$$

The above equations are also derived for the first time in this paper and via the substitution of β_g from (9b) or (9c) gives the early time evolutions of the carrier frequency and wave number. They state that the overall pulse depletion is accompanied by the carrier-frequency (wave-number) down-shift. Furthermore, by putting the obtained equations together with the relation

$(H_{FT}, c\mathbf{K}_F) = H_0(\gamma_g, \gamma_g \mathbf{v}_g)$ and assuming $\beta_g \approx 1$ for early times, we obtain the familiar adiabatic relations $H_{FT}(t)/\omega_0(t) = \text{constant}$ and $K_F(t)/k_0(t) = \text{constant}$. These equations have similarities with the adiabatic equation obtained in Ref. [4] via the SEA. This coincidence is natural as the validity of these equations is restricted to early times or to very weak wake excitations. And they are obtained under the ignorance of group velocity variations (setting $\beta_g = 1$ in Eq.(10) for $\omega_0(t)$), implicitly assumed by the SEA.

According to the early time, adiabatic equation, $H_{FT}(t)/\omega_0(t) = \text{constant}$, and the electromagnetic energy relation in terms of a_0 and ω_0, $H_{FT}(t) = \eta(t) a_0^2(t) \omega_0^2(t)$, we obtain $\eta a_0^2 \omega_0 = \text{constant}$ where η is the pulse shape factor. As long as the pulse shape has not changed seriously ($\eta(t) \approx \eta(0)$), we obtain $a_0^2(t) = a_0^2(0)\omega_0(0)/\omega_0(t)$ which predicts the amplification of the pulse peak amplitude along with the frequency redshift. This amplification observed earlier in Ref. [6] and obtained in relation with wake-amplitude amplification in Refs. [3, 8].

As a remark, it should be stated that the group velocity calculated in Ref. [15], is base on the definition $v_{gt} = S_t / U_t$ where $S_t \equiv \int \mathrm{dx}[c^2 g_x + m_e c^2 \gamma_e n_e v_{ex}]$ and $U_t = \int \mathrm{dx}[u_{EM} + m_e c^2 \gamma_e n_e]$ are respectively the total-energy flux and the total energy. This definition gives a time-independent value for the group velocity as

total energy and momentum are constant. And despite to our definition (Eq. 8), v_{gt} does not coincide with the averaged plasma-wave phase velocity and may be of less interests in applications.

C. COMPARISON WITH SIMULATIONS

Using a 1D3V PIC code written by the author [20-21], many PIC simulations have been performed in order to understand the system behavior at different applied physical parameters. These simulations show precise agreement with our analyses for pulse lengths shorter than the plasma wave length (LWFA regime). Two simulation instances are chosen to be presented in this study. In the first and the main case, say *S1*, the laser wavelength, amplitude and duration are respectively set to $\lambda = 1\mu m$, $a_0 = 2$ and $\tau_L = 60[\text{fs}]$, and the pulse shape is initially sinusoidal. The pulse duration approximately satisfies the resonance condition, i.e. $L_p = c\tau_L \approx \lambda_{\text{p}}^{\text{NL}} / 2$ (L_p is the pulse length and $\lambda_{\text{p}}^{\text{NL}}$ is the relativistic, nonlinear plasma wavelength [2, 16]). The initial plasma profile is step-like with the initial density $n_{e0} / n_c = 0.01$ ($n_c = \varepsilon_0 m_e \omega_0^2 / e^2$ is the critical density), and the initial electron and ion temperatures are set to $k_B T_e / m_e c^2 = 10^{-4} (\sim 50\text{eV})$ and $k_B T_i = 0$ (k_B is Boltzmann constant), respectively. The size of simulation box is 600 λ, with open boundary conditions being applied at its ends for the fields and particles. Each mesh cell is λ/200 long and initially contains 64 macro-particles. Plasma is

initialized in the position range $[40\lambda, 960\lambda]$ and the total simulation run time is set as $t = 3\text{ps}$. In the second and the auxiliary case, say *S2* , every parameter is identical to *S1* except for the pulse length which is set to $\tau_L = 300[\text{fs}]$ and larger than the plasma wavelength. This latter is referred only through Sec. V and for demonstrating the differences predicted by the theory between the long and short pulses.

Our PIC codes are equipped with utilities for detailed spectral and plasma dispersion analyses. Moreover, another utility is implemented to calculate the *adiabatic solution* for the plasma wave at each desired time moment. This utility uses the *instantaneous* vector-potential profile extracted from the direct PIC simulations to derive the QSA solution of Eqs. (1a-1c) at any desired time. Since, this approach is equivalent to treat the time argument of a_y as a parameter in the PCM frame, it gives the adiabatic solution, i.e. the pulse is assumed time-independent during a small time period which is still sufficient for the plasma to pass a plasma wavelengths.

A brief overview of the spatiotemporal evolutions of the laser pulse and the plasma wave in the case of $\tau_L = 60[\text{fs}]$ is presented on Fig. 1. Here, on the left panels (a-d), four snapshots of the Poynting-vector, $\mathbf{g}$, are plotted at four different times within the light-speed commoving-window. Also, are given at these panels

the initial profile of $\mathbf{g}$ (for the comparison purpose) and the corresponding profile of the local wake magnitude, C_w (with reversed sign and shifted by 1, for clarity) described below Eq. (6b). The right panels (e-h) show the longitudinal electron phase-space in one-by-one correspondence with the radiation plots of the left panels. In addition to simulation results, the respective adiabatic solutions are also presented in panels (e-h).

Comparison between the C_w and $\mathbf{g}$ curves in panels (a-d) of Fig. 1 shows that the laser pulse generally experiences the down-chirp in the locations of positive wake excitation (positive gradient of C_w-envelope) and vise versa in the locations of the negative wake excitation (negative gradients of C_w-envelope). Also it is observed that the radiation flows in the opposite direction of gradient of C_w-envelope, being accumulated at descents of this envelope and eroded in their neighborhoods. These observations qualitatively confirm Eqs. (6a) and (6b) supporting the suggestion of the C_w-envelope as an effective, commoving potential for the radiation. Also, it is observed that the radiation is totally decelerated and is more and more displaced negatively inside the light-speed commoving window as time proceeds.

Excellent agreement is observed on Figs. (1e-1h), between the adiabatic and the real solutions for the plasma wave in the radiation region. The exception is small

deviations displayed in the last plot (h) at very long times. Note that, the a_y profile used in the adiabatic solution contains all evolutions up to the plot time. An important feature of this agreement is the local equality between the phase-velocities of the laser pulse and the electron plasma-wave pointed out at the end of Sec. III. Otherwise, we should have observe, for example, mismatching in corresponding locations or dissimilarities between the shapes of density peaks in different solutions, as the laser would oscillate in the local plasma-wave phase frame and no local Hamiltonian constant, like (3b) or (3d), would be obtained. All the observed agreements are in the support of our assumptions in the beginning of Sec. IV.A.

In Fig. 2, the time histories for the electromagnetic energy-momentum and the wakefield amplitude are presented form simulations with $\tau_L = 60[\text{fs}]$, over the full range of interaction time (up to $t = 3\text{ps}$). Also, are presented the analytical results from integration of Eq. (9a) performed using the simulation results for the time history of E_w. Over a large portion of the selected time range, the wake amplitude grows monotonically, as described in the previous works [3, 6, 8] and also recovered here in the last paragraph of the previous subsection. After this growth phase, the wake amplitude decreases awhile, and afterward it experiences an irregular oscillatory pattern. In the time-interval of regular E_w-variations, excellent

agreement is observed between the simulation and the analysis for the energy-momentum. And, in the irregular region, the agreement between the simulations and the adiabatic results is marginally reduced. The long-term, excellent fit observed between the simulations and analyses in this case despite to the early-time nature of Eq. (9a), indicates that the radiation evolutions in the LPCM frame are very slow, i.e. $K_F\big|_{PCM} \approx 0$. Since the norm of the radiation four-momentum, $H_0^2 = H_{FT}^2 - c^2 K_F^2$, is approximately zero ($H_0^2 = U_{p0}^2 / \gamma_{g0}^2 << H_{FT}^2$), as long as the pulse energy is not largely depleted, H_{FT} / c approximately equals K_F as is observed in Fig. 2.

In Fig. (3a), on the left axis, we have plotted the β_g history both from formula (9c) (constant E_w) and from direct integration of (9b) (variable E_w) for the simulation with $\tau_L = 60[\text{fs}]$ and up to $t = 3\text{ps}$. It is observed that including the E_w-variations is very important. The linear value for the group velocity, including the relativistic mass corrections, is given by $\sqrt{1 - n_{e0} / < \gamma_L > n_{cr}}$ ($< \gamma_L > \equiv \sqrt{1 + a_0^2 / 2}$) and assumes the value 0.997 in the case of our parameters. It is indicated by a blue arrow on the figure. It is seen that β_g anomalously remains very close to the unity and above this linear value over a considerably long time period. In Fig (3a) we also plotted on the right axis the history of the pulse displacement in the light-

speed commoving window, $\Delta\xi = c\int_0^t \beta_g(t')\mathrm{d}t' - ct$, using the β_g values calculated in the presence of the wakefield evolutions (Eq. (9b)).

The precise direct-detection of the small variations in β_g, depicted on Fig. (3a), via PIC simulations is impossible due to the finite grid spacing, i.e. accurate measurement of the changes needs ultra-fine resolution of the space which, in turns, makes the long-term simulations cumbersome. Therefore, direct, instantaneous comparison with simulation results has not been made for this quantity. Nevertheless, the conformation of the analyses in the case of energy-momentum, described on Fig (2), guaranties the validity of the formula (9b). Additionally, the comparison between the formula (10), for the carrier wave-number, and corresponding simulation results can be utilized to further approve Eq. (9b) for β_g. Since, the wave-number is proportional to γ_g (see Eq. (10)), it is very sensitive to β_g variations as does γ_g itself. In Fig (3b), we have plotted the time history for carrier wave-number both from the simulations and the analysis. In the analytical case, we used formula (10) with β_g calculated in the two fashions described just above. It is observed that the including E_w-variations, noticeably increases the accuracy of the analytical result at long times. All plotted curves, in Fig (3b), excellently merge at early times and a very good agreement is found

between the direct simulations and analytical results over noticeable portion of the simulation time, all in the favor of Eqs. (9b) and (9c).

V. THE ORIGIN OF ANOMALIES AND THE PLASMA DISPERSION

A. GENERAL CONSIDERATIONS

In this section, we aim to describe the origin of anomalies obtained in the previous section concerning behaviors of the group and phase velocities of light. It has been turned out that these velocities equal locally while in the commonly accepted linear theory the phase velocity of the electromagnetic modes is always larger than their group velocity. In addition, the group velocity (9c) is obtained higher than the linear value and does not tend to this value in the limiting case of very weak wake amplitudes. To answer these questions, we should turn to the detailed analyses of the wave equation and the plasma dispersion in the fully nonlinear regime considered here. The group-velocity behaviors and the resultant central-mode equation (10) suggest the emergence of a new anomalous dispersion-branch with the relation $\omega = (\beta_g / \beta_{g0})ck$ (obtained by dividing expressions for ω_0 and k_0 in Eq. (10)) in the nonlinear regime. This dispersion relation is also consistent with the equal phase and group velocities. Now, the main question is if the wave equation in the presence of relativistic wake excitation by ultra-short pulse allows for such a dispersion branch. And, if the anomalies with respect to the

common theory cease in the case of long pulse with the pulse length and the envelope scale-length larger than the plasma wavelength, initially producing weak wake-amplitudes.

In this section the wave equation (1d) in the light polarization direction is considered in the LPCM frame,

$$\left\{[\frac{\partial^2}{\partial x^2}-\frac{1}{c^2}\frac{\partial^2}{\partial t^2}]a_y=\frac{\Omega^2}{c^2}a_y\right\}_{PCM}. \qquad (11)$$

where $\Omega^2 \equiv \omega_p^2 n_e / n_{e0}\gamma_e$. The full solution and interpretation of behaviors of this wave equation is quite complicated and elaborated. The complexity arises mainly due to the fact that Eq. (11) is a nonlinear differential equation, i.e. right hand side of (11), is not a simple restoring term in the form $F(x,t)a_y$ (as in the case of a preformed density profile), but Ω^2 includes complex dependencies on a_y. Through these dependencies, different electromagnetic modes are coupled to each other, causing complexity of the plasma dispersion. In the quasi-linear regime, this phenomenon results in the parametric instabilities [24]. In the fully nonlinear regime, considered here, the plasma dispersion is not easily understood and the problem is much more involved. We only can argue that appearance of the new dispersion branch is possible and elucidate the essential differences of the linear

and fully nonlinear regime. Our statements will find their final approval from PIC simulations performed at both short and long pulse lengths.

The possibility of the new dispersion branch may be investigated by examining the wave equation (11) against the substitution of the following trial solution,

$$a_y = a_{y.l} + a_{y.h}\,, \tag{12a}$$

with the assumption $\left|a_{y.h}\right| << \left|a_{y.l}\right|$ where l and h indices mean low and high frequency components respectively. By low-frequency (high-frequency) we mean the spectrum components with time-periods comparable to (much shorter than) the time-scale of wake-field evolutions in the LPCM frame. Using (12a), $\Omega^2(a_y)$ as a functional of a_y can be expanded around $a_{y.l}$ and to the second order in $a_{y.h}$ we obtain,

$$\Omega^2(a_y) = \Omega^2(a_{y.l}) + a_{y.h}\,\partial\Omega^2 / \partial a_y\Big|_{a_{y.l}} + (a_{y.h}^2 / 2)\,\partial\Omega^2 / \partial^2 a_y\Big|_{a_{y.l}} \tag{12b}$$

which can be decomposed into low and high frequency parts. The first term in the right hand side of (12b) is purely low frequency, the second is purely high frequency and the third is mixed. In relation with the third term, one should notice that beating between two high frequency waves has low frequency components. Now, the right hand side of Eq. (11), $\Omega^2(a_y)a_y$, is expanded using Eqs. (12_) and is decomposed into low and high frequency parts. In this way, after neglecting

terms beyond the second order in $a_{y.h}$, the wave equation (11) is decomposed into high and low frequency parts as follow:

$$\left\{[\frac{\partial^2}{\partial x^2}-\frac{1}{c^2}\frac{\partial^2}{\partial t^2}]a_{y.l}=\frac{\Omega_l^2}{c^2}a_{y.l}+L.F.P.\left[\left(\frac{\Omega_l^{2\prime}}{c^2}+a_{y.l}\frac{\Omega_l^{2\prime\prime}}{2c^2}\right)a_{y.h}^2\right]\right\}_{PCM}, \tag{13a}$$

$$\left\{[\frac{\partial^2}{\partial x^2}-\frac{1}{c^2}\frac{\partial^2}{\partial t^2}]a_{y.h}=\frac{\Omega_l^2}{c^2}a_{y.h}+a_{y.l}\frac{\Omega_l^{2\prime}}{c^2}a_{y.h}+H.F.P.\left[\left(\frac{\Omega_l^{2\prime}}{c^2}+a_{y.l}\frac{\Omega_l^{2\prime\prime}}{2c^2}\right)a_{y.h}^2\right]\right\}_{PCM} \tag{13b}$$

where $\Omega_l^2\equiv\Omega^2(a_{y.l})$, $\Omega_l^{2\prime}\equiv\partial\Omega^2/\partial a_y\big|_{a_{y.l}}$ and $\Omega_l^{2\prime\prime}\equiv\partial^2\Omega^2/\partial a_y^2\big|_{a_{y.l}}$, and *L.F.P.* and *H.F.P.* are abbreviations for low and high frequency parts respectively.

B. THE LOW-FREQUENCY MODES

The low-frequency modes are described by Eq. (13a). The second term in the right hand side of (13a) introduces coupling between $a_{y.h}$ and $a_{y.l}$. It is a small perturbation and can be ignored in obtaining $a_{y.l}$. Therefore, (13a) reduces to,

$$\left\{[\frac{\partial^2}{\partial x^2}-\frac{1}{c^2}\frac{\partial^2}{\partial t^2}]a_{y.l}=\frac{\Omega_l^2}{c^2}a_{y.l}\right\}_{PCM} \tag{14}$$

Note that, $\Omega_l^2=\Omega^2(a_{y.l})$. This equation has the form of the original wave equation (11) but with the peculiarity that $a_{y.l}$ is forced to oscillate with the frequency near the inverse time-scale of the self-consistent profile Ω_l^2.

In order to better understand the significance of the above mentioned peculiarity of low-frequency modes, let present the formal mode-space (ω,k) presentation of Eq. (14). The commonly used Laplace method is utilized for time transformation in the presence of initial conditions. In this method, the wave equation is multiplied by $e^{i\varpi t}$ and then integrated over the time-domain. Here, we customarily take the transformation parameter as $i\varpi$. Applying this transformation, after some mathematical manipulations (14) is converted to (see e.g. [22], Sec. 15.10, example 15.10.2),

$$\left\{[\frac{\partial^2}{\partial x^2}+\frac{\varpi^2}{c^2}]\tilde{a}_y(x,\varpi)=\frac{1}{c^2}\int_C \mathrm{d}\varpi'[\tilde{\Omega}^2(x,\varpi-\varpi')\tilde{a}_y(x,\varpi')]+I(x;\varpi)\right\}_{PCM} \qquad (15)$$

where $\tilde{Q}(x,\varpi)=(2\pi)^{-1/2}\int_0^\infty \mathrm{dt}[Q(x,t)e^{i\varpi t}]$ shows the Laplace-transform of the quantity $Q(x,t)$, and $I(x;\varpi)=-c^{-2}[\partial a_y/\partial t-i\varpi a_y]\big|_{t=0}$ represents the initial conditions with parametrical dependence on ϖ. The inverse transform of quantity $Q(x,t)$ is given by,

$$Q(x,t)=\frac{1}{\sqrt{2\pi}}\int_C \tilde{Q}(x,\varpi)e^{-i\varpi t}\mathrm{d}\varpi \qquad (16)$$

where the integration path *C* lies in the upper half of complex ϖ-plan and parallel to the real axis, keeping all $\tilde{Q}(x,\varpi)$-singularities on bellow. It may be completed

by a semi-circle with infinite radius in the lower half of the complex ϖ-plan (see Jackson [23], Sec. 12.11). Such treatment of singularities is equivalent to application of causal boundary conditions.

The mode-space presentation of (14) is completed by Fourier-transform of (15). To obtain this transform, Eq. (15) is multiplied by e^{-ikx} and is integrated over the space. And after some mathematical manipulations and applying boundary conditions $\partial\tilde{a}_y(x,\varpi)/\partial x\Big|_{x=\pm\infty} = \tilde{a}_y(x,\varpi)\Big|_{x=\pm\infty} = 0$, we obtain,

$$\left\{(\varpi^2 - k^2c^2)\hat{a}_y(k,\varpi) = c^2\hat{I}(k;\varpi) + \int_C \mathrm{d}\varpi' \int_{-\infty}^{\infty} \mathrm{dk}'[\hat{\Omega}^2(k-k',\varpi-\varpi')\hat{a}_y(k',\varpi')]\right\}_{PCM} \quad (17)$$

where $\hat{Q}(k,\varpi) = (2\pi)^{-1/2}\int_0^{\infty}\mathrm{dx}[\tilde{Q}(x,\varpi)e^{-ikx}]$ shows the Fourier transform of quantity $\tilde{Q}(x,\varpi)$. Note that, since the forms of Eqs. (11) and (14) are identical, expression (17) can be applied without changes about the general wave equation (11). The case with $\hat{\Omega}^2(k,\varpi) = \omega_p^2\delta(k)\delta(\varpi)$ corresponds to a time and space independent plasma density, occurs in the common linear regime. In this case the common electromagnetic dispersion relation is recovered.

The preformed, static density profile corresponds to $\hat{\Omega}^2(k,\varpi) = \omega_p^2 F(k)\delta(\varpi)$ where $F(k)$ is the density shape-factor in the Fourier space. The ordinary generalized form of this case corresponds to the quasi-linear treatment of the

radiation in the presence of a preformed density profile, showing the related parametric instabilities [25]. At these conditions the general form of $\hat{\Omega}^2(k,\varpi)$ is,

$$\hat{\Omega}^2(k,\varpi) = \omega_p^2 F_0(k)\delta(\varpi) + \varepsilon\omega_p^2 F_1(k,\varpi) \qquad (18)$$

where F_0 and F_1 are two definite functions, and ε is a small perturbation parameter.

In order to understand the significance of commensurability of the considered low-frequencies with the inverse time-scale of Ω_l^2, it is worthwhile to notice the opposite situation for which the radiation frequency in Eq. (17) satisfy $\varpi >> \varpi''$ with $\varpi'' = \varpi - \varpi'$. Under this condition the frequency dependent part of $\hat{\Omega}^2(k,\varpi)$ can be approximated by a δ-function and whereby the ordinary case of Eq. (18) is recovered. Therefore, the extra-ordinary behaviors of the low-frequency modes are owing to the self-consistent, commensurable time-evolutions of the involved density profile in the LPCM frame. Under these conditions the mode-space presentation (17) becomes highly non-linear and non-invertible, causing the ordinary plasma mode concept loses its applicability. The radiation evolution in the mode-space presents the full nonlinear analogous of the parametric instabilities with the extra-ordinary condition on the growth (damping) rates -for each mode of $a_{y.l}$ spectrum we have $\varpi = \varpi_r + i\Gamma$ with Γ comparable to ϖ_r despite to the ordinary quasi-liner problems. The growth and damping rates of different modes

cannot be calculated analytically but overall evolutions should satisfy the conservation laws (6).

Since, according to the local conservation laws (6) the radiation energy is totally conserved in the LPCM frame while the radiation momentum changes both locally and totally, the mode-space evolutions occur only along the wave-number axis in the LPCM frame, i.e. for a newly produced mode in the LPCM frame, $(\omega_n, k_n)\big|_{PCM}$, we have $\omega_n\big|_{PCM} = \omega_i\big|_{PCM}$ and $k_n\big|_{PCM} = [k_i + \Delta k]\big|_{PCM}$. Here, Δk is the wave-number shift introduced by the local momentum change, and, ω_i and k_i are the original (pump) frequency and wave number. Using Lorentz transformations for (ω, k), we obtain in the laboratory frame,

$$k_n = k_i + \gamma_g \Delta k\big|_{PCM}. \tag{19a}$$

$$\omega_n = \omega_i + \gamma_g c\beta_g \Delta k\big|_{PCM}. \tag{19b}$$

Since the wake-excitation is of local nature described by position dependent C_W, Δk assumes a range of values corresponding to different Fourier components of the curve $\partial C_W / \partial x$. Therefore, it is generally expected that in addition to down-shift, the spectrum undergoes broadening along the *k*-axis without explicit dependence on the shape of plasma density profile in the Fourier space. This reflects the fact that the right hand side of (14) is not a restoring term in this case. More importantly, it is turned out that spectral evolutions occur along the linear

curve $\Delta\omega_{fi} = c\beta_g \Delta k_{fi}$ in the laboratory frame. Using this equation together with the fact that initially the radiation satisfies the vacuum dispersion $\omega = ck$, if the small group velocity variations be ignored we find that the low-frequency modes are governed by,

$$\omega = ck . \tag{19c}$$

C. HIGH FREQUENCY MODES

The high frequency components are governed by Eq. (13b). Since $\Omega_l^2 \equiv \Omega^2(a_{y.l})$ and $\Omega_l^{2\prime} \equiv \partial\Omega^2 / \partial a_y\big|_{a_{y.l}}$ are approximately static in the presence of considered high-frequencies, and are independent of $a_{y.h}$, the problem reduces to the solution of a weakly nonlinear wave equation in the presence of a preformed density profile with the local plasma-frequency $\Omega_p^2(x) = \Omega_l^2 + a_{y.l}\Omega_l^{2\prime}$. The weak nonlinearity is introduced via the third term in the right hand side of (13). Here, we do not go through the full discussion of this nonlinearity, being satisfied of the comment that it causes different modes to be converted to each other. The reduced form of (13b) is,

$$\left\{ [\frac{\partial^2}{\partial x^2} - \frac{1}{c^2}\frac{\partial^2}{\partial t^2} - \frac{\Omega_p^2(x)}{c^2}] a_{y.h} = 0 \right\}_{PCM} . \tag{20}$$

The Laplace-transform of the wave equation (20) results in,

$$\left\{[\frac{\partial^2}{\partial x^2}+\frac{\varpi^2-\Omega_p^2(x)}{c^2}]\tilde{a}_{y.h}(x,\varpi)=\tilde{I}(x;\varpi)\right\}_{PCM} \tag{21}$$

To obtain a formal solution to Eq. (21), a proper generalization of the Fourier-transform is considered (see e.g. [22], Sec. 10.5); the solution and the right-hand side of Eq. (21) is expanded in terms of eigen-functions of the self-adjoint operator $O_0=\partial^2/\partial x^2+[\omega_p^2-\Omega^2(x)]/c^2$. The reason for choosing this operator will become soon clear. To obtain the corresponding transform of Eq. (21), we consider $u_\xi(x)$, the eigen-function of O_0 corresponding to the eigen-value of ξ^2,

$$\left\{\left(\frac{\partial^2}{\partial x^2}+\frac{\omega_p^2-\Omega_p^2(x)}{c^2}\right)u_\xi+\xi^2u_\xi=0\right\}_{PCM}, \tag{22}$$

then Eq. (21) is multiplied by $u_\xi^*(x)$, the complex-conjugate of $u_\xi(x)$, and afterward is integrated over *x*. After some mathematical manipulations and applying boundary conditions $\partial\tilde{a}_{y.h}(x,\varpi)/\partial x\big|_{x=\pm\infty}=\tilde{a}_{y.h}(x,\varpi)\big|_{x=\pm\infty}=0$, we obtain,

$$\left\{\hat{a}_{y.h}(k,\varpi)=\frac{c^2\hat{I}(\xi;\varpi)}{\varpi^2-\omega_p^2-\xi^2c^2}\right\}_{PCM} \tag{23}$$

where $\hat{I}(\xi;\varpi)=\int_{-\infty}^{\infty}\mathrm{d}x[u_\xi^*(x)I(x;\varpi)]$ and $\hat{a}_{y.h}(\xi,\varpi)=\int_{-\infty}^{\infty}\mathrm{d}x[u_\xi^*(x)\tilde{a}_{y.h}(x,\varpi)]$. The reason for choosing O_0 in the above procedure is now clear; Eq. (23) takes a simple form similar to the relation in the absence of spatial-variations of $\Omega_p^2(x)$, and all

differences go into the new transform of $I(x;\varpi)$, say $\hat{I}(\xi;\varpi)$. This procedure of changing the expansion basis functions from ordinary Fourier phasors to u_ξs, makes the full transformation invertible.

Now, time and space transformations are inverted by putting (23) into the inverse of used transformations and we obtain,

$$\left\{ a_{y.h}(x,t) = \frac{1}{\sqrt{2\pi}} \int_C \mathrm{d}\varpi \left[e^{-i\varpi t} \int_{\text{continuum}} \mathrm{d}\xi [\frac{\hat{I}(\xi;\varpi) u_\xi(x)}{\varpi^2 - \omega_p^2 - \xi^2 c^2}] + \sum_{\text{discrete}} [\frac{\hat{I}(\xi;\varpi) u_\xi(x)}{\varpi^2 - \omega_p^2 - \xi^2 c^2}] \right] \right\}_{PCM} \quad (24a)$$

which is the formal solution of $a_y(x,t)$ in terms of the initial conditions. ξ-integrals are performed over the all values in the continuum part of the eigen-value spectrum of O_0 and sigma corresponds to the discrete part. Assuming no singularity and multi-valuedness in $\hat{I}(\xi;\varpi)$, after performing the ϖ integral by treatment of singularities at $\varpi = \pm\omega_\xi = \pm\sqrt{\omega_p^2 + c^2\xi^2}$, the above expression simplifies to,

$$\begin{aligned} a_{y.h}(x,t)\big|_{PCM} = -i\sqrt{2\pi}c^2 \left\{ \int_{\text{continuum}} \mathrm{d}\xi \left[\frac{u_\xi(x)}{2\omega_\xi} \left(\hat{I}(\xi;\omega_\xi) e^{-i\omega_\xi t} - \hat{I}(\xi;-\omega_\xi) e^{+i\omega_\xi t} \right) \right] \right\}_{PCM} \\ -i\sqrt{2\pi}c^2 \left\{ \sum_{\text{discrete}} \left[\frac{u_\xi(x)}{2\omega_\xi} \left(\hat{I}(\xi;\omega_\xi) e^{-i\omega_\xi t} - \hat{I}(\xi;-\omega_\xi) e^{+i\omega_\xi t} \right) \right] \right\}_{PCM} \end{aligned} \quad (24b)$$

In the presence of the complex form of $\Omega_p^2(x)$ in our problem, the analytical form of $u_\xi(x)$ cannot be obtained. Nevertheless, the important properties of the formal solution (24) can be described by noting that Eq. (22) is the time

independent Schrödinger equation well discussed in text books (see. e. g. [26]). In this picture, ω_ξ and $\Omega_p^2(x)$ take the role of the total and the potential energies respectively. The wave-number, k, takes the role of momentum, corresponding to the operator $i\partial/\partial x$. Since, this operator does not commute with O_0, no one-to-one relation exists between ω_ξs and k^2s. Therefore, the common sense concept of dispersion relation in terms of k is lost. Nevertheless, the role of k is played by ξ and certain conditions exist over the ω_ξ values; for every ξ, ω_ξ^2 should be larger than minimum of $\Omega_p^2(x)$. If $\Omega_p^2(x)$ include descents in its profile, as in our problem, the discrete part of spectrum (the second term in the right hand side of (24b) is populated and local peaks appear in the $\omega - k$ plan. Due to incommutability of $i\partial/\partial x$ and O_0 each ω corresponds many values of k and vice versa. Therefore the produce spectrum is expected to be broadened over k and (or) ω space, depending on the initial conditions. We should notice that despite the low-frequency modes, here, the spectrum evolutions are directly determined by the shape of the density profile in the Fourier space.

D. COMPARISON WITH PIC SIMULATIONS

The strict decomposition of high and low frequency modes considered in above description does not necessarily occur in reality. Nevertheless, the radiation behavior can be considered as an unknown mixture of these mentioned two cases.

It is expected that extra-ordinary behaviors cease in the favor of ordinary ones at weak wakefield amplitudes occurred at long pulse lengths. Therefore, in addition to demonstrating the obtained results, it is worthwhile to present and compare the simulation results for dispersion behavior at long pulse lengths.

In the case of long pulse length the wakefield dynamics is essentially different. In Fig.4 two instances of the wakefield profile within the commoving window are presented at two different times, t=0.6ps and t=2.7ps form the simulation with the long pulse length, $\tau_L = 300\text{fs}$. In addition, the comparison with the adiabatic solution is made and the corresponding snap-shots of vector potential are given. These data help us to briefly understand the differences of wake excitation in the case of long pulse with respect to the ultra-short pulse. The full discussion of this issue is elaborated and out of the scope of this work. Shortly speaking, in the case of long pulse, the wakefiled is initially weak despite the ultra-short pulse (see panel (a)). Instead, an initial space-charge is formed in the pulse region during crossing of the plasma-boundary by the pulse, and due to the off-phase propagation of the boundary-originated thermal electrostatic-modes with the laser pulse (see panel (a)). Afterward, this disturbance is amplified by the modulation instability (see panel (b)). It is observed that the adiabatic and the simulation results for the wakefiled profile do not coincide generally. At long times, the coincidence

improves but, nevertheless, the deviation is still presented in the back parts of the pulse region.

The temporal evolution of the vector-potential (a_y) spectral-density is given in Fig. 5 form both simulations with $\tau_L = 60,\ 300\text{fs}$ (a, c). In addition the corresponding long-term appearance of the potential together with its initial profile is plotted for each simulation (b, d). For $\tau_L = 60\text{fs}$, it is obviously observed that the central wave-number, k_0, continuously decreases along with the spectral-broadening increase. The spectrum takes a very broad shape almost decreasing with the wave-number (maximum at zero) at very long times. Accordingly, a tail of large length periods appears in the long-term profile of vector potential. In the case of $\tau_L = 300\text{fs}$, on the other hand, the central wave-number does not display noticeable continuous down-shift. In the initial stages (see plot at *t*= 0.9ps), the radiation seems to undergo scatterings with nearly uniform distribution over the *k*-domain. Most-likely, this phenomenon is related to the plasma-chaos [14] (formation of incoherence space-charge mode) during the laser entrance, which in turns produces Thomson-like scatterings. Afterward, the radiation experiences the so-called electromagnetic cascading [27-28], with appearance of spectrum peaks displaced from the central mode by nearly multiples of plasma wave-number $k_p \approx c/\omega_p = 0.1k_{00}$ ($k_{00} = k_0(t=0)$). Especially, it is observed that that at long-

times (t=1.8ps and t=2.7ps) when the boundary effects becomes stabilized, the initial central mode diminishes and then is eliminated, and the scattered mode at $k_{00} - k_p$ becomes dominant.

Observations on Fig. 5 indicate that the slow-mode population of the spectrum is dominant in the case of ultra-short pulse, $\tau_L = 60\text{fs}$, and is weaker in the case of long pulse, $\tau_L = 300\text{fs}$, in agreement with different involved wake amplitudes. In the latter case the overall pulse deceleration is weaker due to the absence of the initial strong wake excitation, therefore the right-hand side of wave equation (11), reveals its restoring nature more strongly, in the sense discussed in the previous subsections. In this case, despite to the case of $\tau_L = 60\text{fs}$, the spectrum shape at long times is directly affected by the Fourier transform of the periodic density profile(not shown here, but can be inferred from wakefiled profile on Fig. (4b)) by manifesting the so-called cascading [27-28] predicted here by the discrete part of formula (24b). This phenomenon is in agreement with descriptions given above Eq. (19c) and below Eq. (24b).

In Fig 6, we have plotted the dispersion relation at three different time instances form both simulations, $\tau_L = 60\text{fs}\,(\text{top})$ and $\tau_L = 300\text{fs}\,(\text{bottom})$. Since both dispersion curves $\omega^2 = \omega_p^2 + c^2k^2$ and $\omega = ck$ merge at large k-values, in order to distinguish the different dispersion behaviors it is necessary to detect small k-

values. Small *k*-values appear at long times due to the plasma wave-steepening. The data at long times (panels (c, f)) indicate that in the case of ultra-short pulse, the linear dispersion curve (Eq. 19c) is ultimately dominant while in the case of long pulse the common electromagnetic dispersion $\omega^2 = \omega_p^2 + c^2 k^2$ takes a significant role. These observation, again, confirm our theory outlined in the previous subsections. For both cases it is clearly observed that the radiation undergoes very large evolutions along the dispersion curves, an expected character of the fully nonlinear regime.

At the end it is worthwhile to notice that the deviations observed at long times between PIC results of Sec IV.C, on Fig.(3b), in the case of Eqs (10) and (9b), are related to the missing of the simple relation $(H_{FT}, c\mathbf{K}_F) = H_0(\gamma_g, \gamma_g \mathbf{v}_g)$ supposed in Sec IV.B between the total energy and momentum of the radiation. This missing is due to the onset of local effects with the manifestation of spectral broadening described above (Figs. 5 and 6). In fact, the assumed simple relation, $(H_{FT}, c\mathbf{K}_F) = H_0(\gamma_g, \gamma_g \mathbf{v}_g)$, is valid until the central mode does not perform jump and its population is dominant over the full spectrum. This is while the broadening highly develops at long times (see Fig. (5a) at $t = 1.8\text{ps}$ and $t = 2.7\text{ps}$). Specially, as displayed on Fig. (3b), the spectrum peak experiences a sudden jump in the carrier wave-number around the normalized time 4000 due to the strong phase-

modulation in the steepened wake excitation profile. Consistently, the calculated pulse displacement (via Eq. (9b)) in the commoving window, $\Delta\xi$, displayed on Fig. (3a), deviates from the direct simulation results presented on Fig. 1; the maximum calculated value is $\Delta\xi(t=3\text{ps})=-1.6\mu\text{m}$ (Fig. 3a) while the pulse concentration is displaced by more than $-5\mu\text{m}$ at the end, as seen in Fig. (1d).

VI. CONCLUSION

In conclusion, we have solved the long-lasting problem of the group velocity behaviors in LWF and outlined the complex nonlinear plasma physics behind it. The anomalously behaved ultra-high group velocities demonstrated in this work, indicate that the wave-break amplitude is not much affected by the pulse group velocity despite the commonly believed opinion (see e.g. Ref. [2]). Instead, phase-velocity decrease due to the plasma wave-length lengthening behind the pulse described in [3] may dominantly affect the wave-break. At high plasma densities, our results provide a basis to understand the observed pulse slow-down [29] and the radiation evolutions causing the electron acceleration and plasma heating [11-14]. From the fundamental-plasma perspective, new physical insights are obtained into the nonlinear plasma dispersion under the propagation of intense short light pulse. Demonstrating a new anomalous dispersion branch in this regime, may

stimulate many fundamental researches and open a new avenue in the field of the nonlinear plasma electrodynamics.

FIGURE CAPTIONS

Figure 1(Color online)**:** (For $\tau_L = 60\,fs$) Left panels show the profiles of Poynting vector (blue) and local wake-excitation with reversed sign and shifted by 1 (orange) at four different times t=0.9ps (a), t=1.8ps (b), t=2.4ps (c) and t=3ps (d) -in addition the initial Poynting vector (green) is shown in each panel. Right panels show the longitudinal phase space in one-by-one correspondence with the left panels from simulations (black points) and the adiabatic solution (red dash-dot lines).

Figure 2(Color online)**:** (For $\tau_L = 60\,fs$) Time histories of the electromagnetic momentum (K_F) (red-star line), electromagnetic energy (H_{FT}) (black-cross line), wakefield amplitude (E_w) (green-solid line) and electromagnetic momentum (K_F) form time-integration of Eq. (9a) (blue-solid line). The maximum normalized-time corresponds to $t = 3$ps and ω_{00} means $\omega_0(t=0)$.

Figure 3(Color online)**:** (For $\tau_L = 60\,fs$) Time history of the group velocity (left axis) from formula (9c) with constant-E_w (red-dashed line), from direct integration of (9b) with variable-E_w (black-solid line) and from the linear theory (blue arrow), and the calculated pulse displacement (green- solid line, right axis) (a). Time history of the carrier wave-number from simulations (orange- cross line), and from analytic Equation (10), with β_g being calculated in two fashions described just above, constant-E_w (red-dashed line) and variable-E_w (black-solid line) (b). The maximum normalized-time corresponds to $t = 3$ps .

Figure 4(Color online**):** The wakefield profile (left axis) from direct simulation (black-solid line) and adiabatic (Ad) solution (red-dashed-dot line) and the vector potential profile (right axis, blue-broken line) for $\tau_L = 300\,fs$, at t=0.6ps (a) and t=2.7ps (b).

Figure 5(Color online**):** Spectral density of the vector potential (a_y) vs normalized wave number and the potential vs *x* from simulations with $\tau_L = 60\,fs$ (left) and $\tau_L = 300\,fs$ (right). The spectral density (a, c) is plotted at four moments, *t*=0.0 (green-dashed line), *t*=0.9ps (red-solid line), *t*=1.5ps (cyan-solid line) and *t*=2.7ps (black-solid line), and the potential (b, d) at two moments *t*=0.0 (green-dashed line) and *t*=2.7ps (blue-solid line). k_{00} means $k_0(t=0)$.

Figure 6(Color online)**:** Dispersion relation from simulations with $\tau_L = 60\,fs$ (top) and $\tau_L = 300\,fs$ (bottom) at three different times *t*=0.9ps (a, d) , *t*=1.8ps (b, e) and *t*=2.7ps (c, f). In the onset of panel (c, f) the plot is magnified in the given range and the broken lines are the dispersion relations, $\omega = ck$ (red) and $\omega^2 = ck^2 + \omega_p^2$ (black).

REFERENCES

[1] G. A. Mourou, T. Tajima and S. V. Bulanov, **Rev. Mod. Phys. 78**, 309 (2006).

[2] E. Esarey, C. B. Schroeder and W. P. Leemans, **Rev. Mod. Phys. 81**, 1229 (2009).

[3] C. B. Schroeder, C. Benedetti, E. Esarey and W. P. Leemans, **Phys. Rev. Lett. 106**, 135002 (2011).

[4] S. V. Bulanov, I. N. Inovenkov, V. I. Kirsanov, N. M. Naumova and A. S. Sakharov, **Phys. Fluids B 4**, 1935 (1992).

[5] C. D. Decker, W. B. Mori, K. C. Tzeng and T. Katsouleas, **Phys. Plasmas 3** 2047 (1996).

[6] D. F. Gordon, B. Hafizi R. F. Hubbard, J. R. Penano, P. Sprangle and A. Ting, **Phys. Rev. Lett. 90,** 215001 (2003).

[7] J. Faure, Y. Glinec, J. J. Santos, F. Ewald, J.-P. Rousseau, S. Kiselev, A. Pukhov, T. Hosokai, and V. Malka, **Phys. Rev. Lett. 95,** 205003 (2005).

[8] B. A. Shadwick, C. B. Schroeder and E. Esarey, **Phys. Plasmas 16**, 056704 (2009).

[9] C. Benedetti, F. Rossi, C. B. Schroeder, E. Esarey and W. P. Leemans, **Phys. Rev. E 92**, 023109 (2015).

[10] Z. Bu and P. Ji, **Phys. Plasmas 19**, 113114 (2012).

[11] Z. M. Sheng, K. Mima, J. Zhang and J. Meyer-ter-Vehn, **Phys. Rev. E 69**, 016407 (2004).

[12] F. Sylla, A. Flacco, S. Kahaly, M. Veltcheva, A. Lifschitz, V. Malka, E. d'Humières, I. Andriyash and V. Tikhonchuk, **Phys. Rev. Lett. 110**, 085001 (2013).

[13] J. H. Bin, W. J. Ma, H. Y. Wang, M. J. V. Streeter, C. Kreuzer, D. Kiefer, M. Yeung, S. Cousens, P. S. Foster, B. Dromey, X. Q. Yan, J. Meyer-ter-Vehn, M. Zepf and J. Schreiber, **Phys. Rev. Lett. 115**, 064801 (2015).

[14] E.khalilzadeh, J.Yazdanpanah, J. Jahanpanah, A.chakhmachi and E.Yazdani, **Phys. Plasmas 22**, 113115(2015).

[15] C. D. Decker and W. B. Mori, **Phys. Rev. Lett. 72,** 490 (1994).

[16] P. Sprangle, E. Esarey and A. Ting, **Phys. Rev. A** 41, 4463 (2004).

[17] See supplemental material A [Here, it is shown that the set of equations (1) can result the covariant conservations laws of equations (2)].

[18] See supplemental material B [Here, it is explicitly shown that the common QSA equations could be obtained by assuming the time-independency in the *real Lorentz boost* LPCM-frame and then transforming the reduced equations into the laboratory].

[19] S. Weinberg, *Gravitation and Cosmology: Principles and applications of general theory of relativity*, (John Wiley & Sons Inc., New York, 1972).

[20] J. Yazdanpanah and A. Anvary, **Phys. Plasmas 19**, 033110 (2012).

[21] J. Yazdanpanah and A. Anvary, **Phys. Plasmas 21,** 023101 (2014)

[22] G. B. Arfken and H. J. Weber, *Mathematical methods for physicists*, 6th Ed., (Elsevier Academic Press, New York, 2005).

[23] J. D. Jackson, *Classical Electrodynamics,* 3rd Ed., (John Wiley & Sons Inc., New York, 1999).

[24] J. F. Drake, P. K. Kaw, Y. C. Lee, G. Schmid, C. S. Liu and M. N. Rosenbluth, **Phys. Fluids 17**, 778 (1974).

[25] M. N. Rosenbluth, **Phys. Rev. Lett. 29**, 565 (1972).

[26] L. D. Landau and E. M. Lifshitz, *Quantum mechanics, nonrelativistic theory*, 3rd Ed., (Pergamon Press Inc., New York, 1977).

[27] S. J. Karttunen and R. R. E. Salomaa, **Phy. Rev. Lett 56,** 604 (1986).

[28] K. C. Tzeng, W. B. Mori and T. Katsouleas, **Phys. Plasmas 6,** 2105 (1999).

[29] T. Iwawaki, H. Habara, T. Yabuuchi,M. Hata, H. Sakagami and K. A. Tanaka, **Phys. Rev. E 92**, 013106 (2015).

FIG. 1

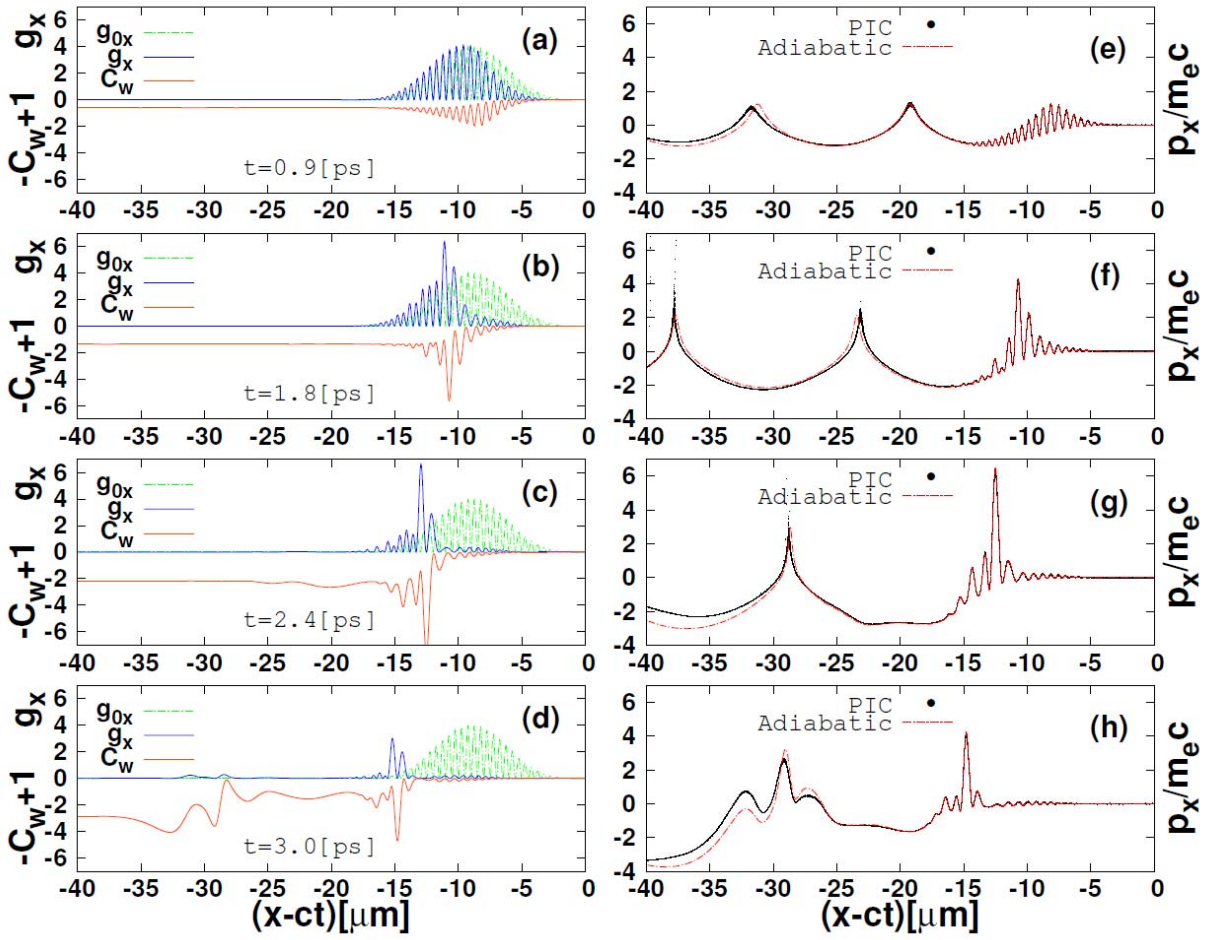
(a)
(b)
(c)
(d)
(e)
(f)
(g)
(h)
g_{0x}
g_x
C_w
$-C_w+1$
g_x
t=0.9[ps]
t=1.8[ps]
t=2.4[ps]
t=3.0[ps]
PIC
Adiabatic
p_x/m_ec
(x-ct)[μm]

FIG. 2

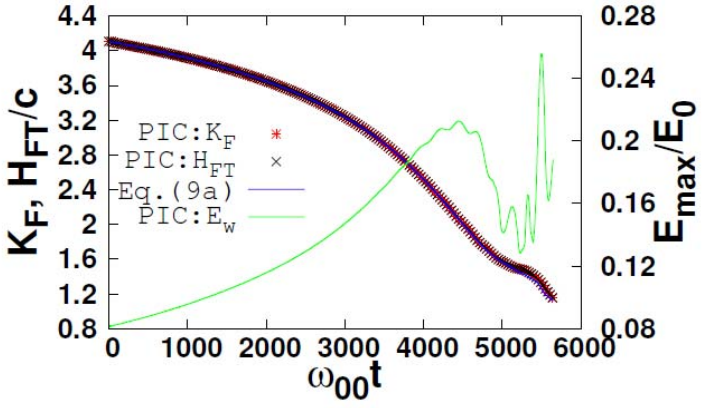
4.4
4
3.6
3.2
2.8
2.4
2
1.6
1.2
0.8
0
1000
2000
3000
4000
5000
6000
$\omega_{00}t$
$K_F, H_{FT}/c$
PIC:K_F
PIC:H_{FT}
Eq.(9a)
PIC:E_w
0.28
0.24
0.2
0.16
0.12
0.08
E_{max}/E_0

FIG. 3

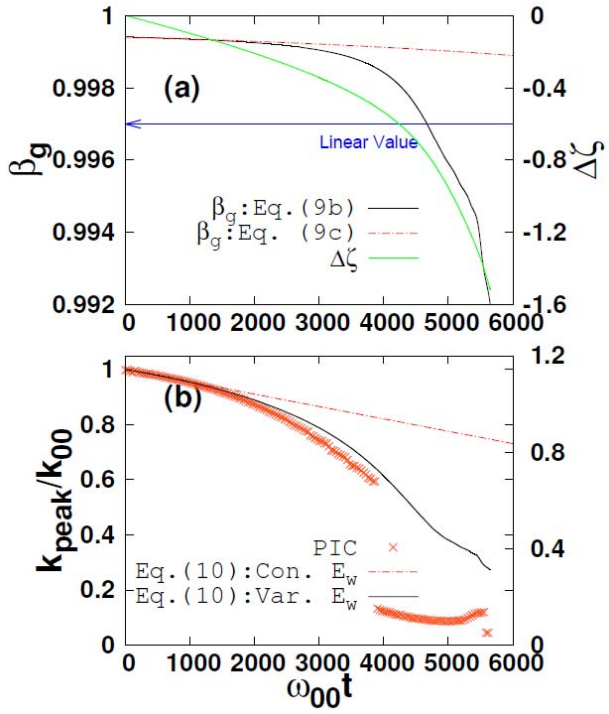
(a)
Linear Value
β_g:Eq.(9b)
β_g:Eq. (9c)
$\Delta\zeta$
β_g
$\Delta\zeta$
(b)
PIC
Eq.(10):Con. E_w
Eq.(10):Var. E_w
k_{peak}/k_{00}
$\omega_{00}t$

FIG. 4

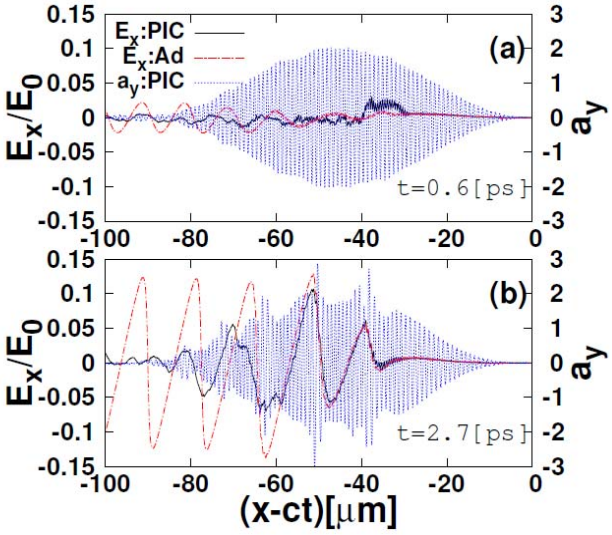

FIG. 5

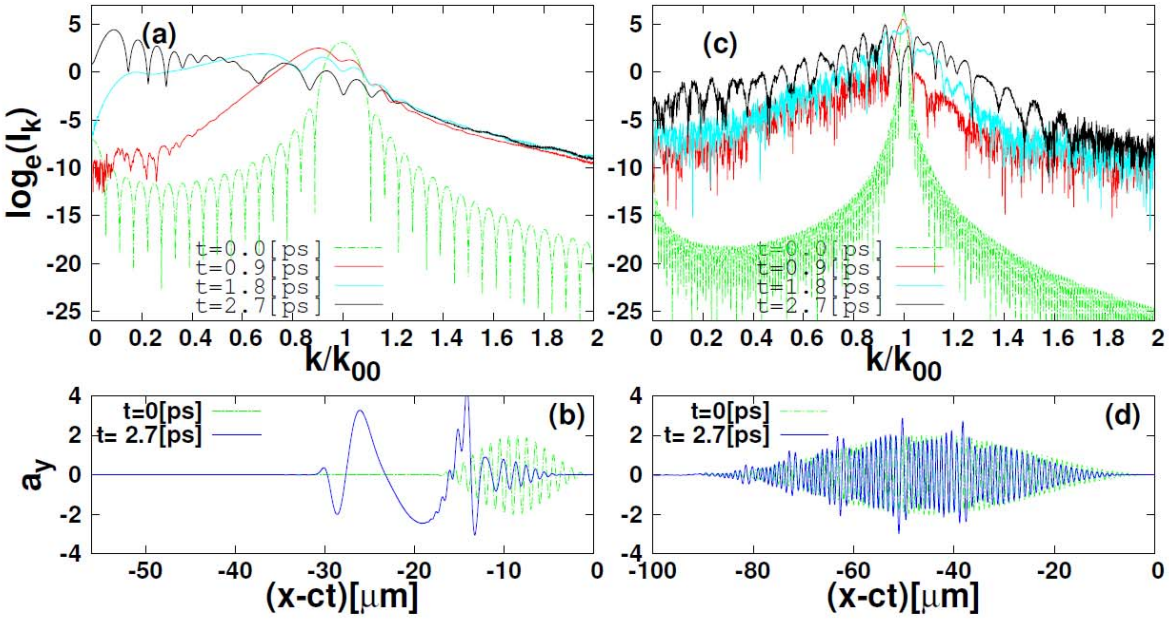
(a)
(b)
(c)
(d)
$\log_e(I_k)$
k/k_{00}
t=0.0[ps]
t=0.9[ps]
t=1.8[ps]
t=2.7[ps]
a_y
t=0[ps]
t= 2.7[ps]
(x-ct)[μm]

FIG. 6

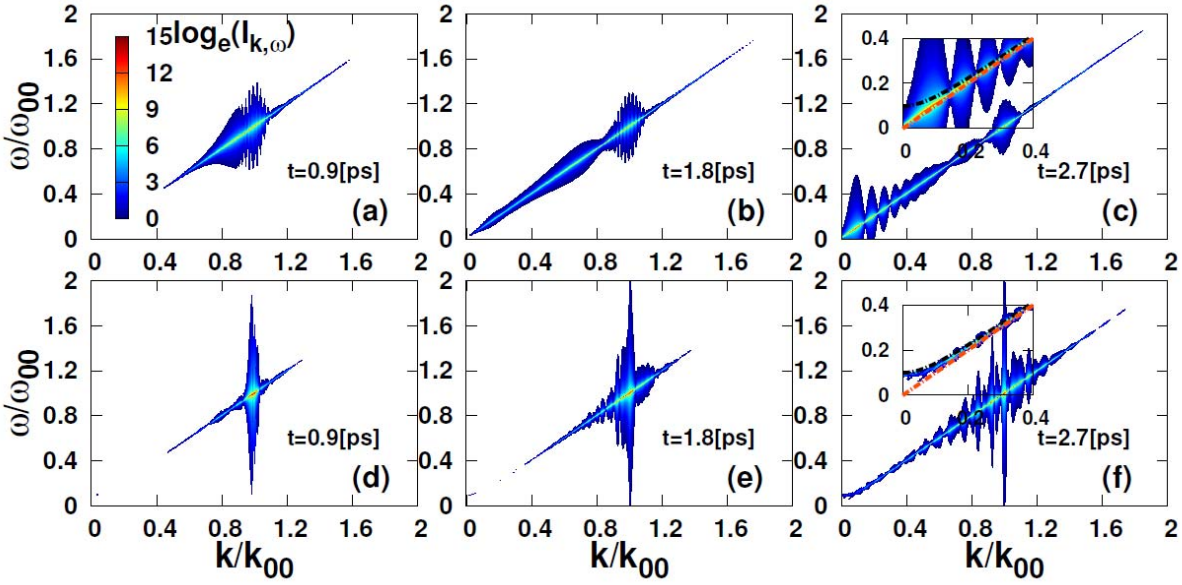
15log_e(I_k,ω)
12
9
6
3
0
t=0.9[ps]
(a)
t=1.8[ps]
(b)
t=2.7[ps]
(c)
t=0.9[ps]
(d)
t=1.8[ps]
(e)
t=2.7[ps]
(f)
ω/ω00
k/k00